© 2001 Nature Publishing Group http://structbio.nature.com

The structure of Pariacoto virus reveals a dodecahedral cage of duplex RNA

Liang Tang[1], Karyn N. Johnson[2], L. Andrew Ball[2], Tianwei Lin[1], Mark Yeager[1,3,4] and John E. Johnson[1]

The 3.0 Å resolution crystal structure of Pariacoto virus (PaV) reveals extensive interactions between portions of the viral RNA genome and the icosahedral capsid. Under the protein shell of the T = 3 quasi equivalent capsid lies a dodecahedral cage composed of RNA duplex that accounts for ~35% of the single-stranded RNA genome. The highly basic N-terminal regions (residues 7–54) of the subunits, forming pentamers (A subunits) are clearly visible in the density map and make numerous interactions with the RNA cage. The C-terminal segments (residues 394–401) of the A subunits lie in channels near the quasi three-fold axes. Electron cryo-microscopy and image reconstruction of PaV particles clearly show the dodecahedral RNA cage.

© 2001 Nature Publishing Group http://structbio.nature.com

Pariacoto virus (PaV) is a single-stranded RNA virus recently isolated in Peru from the Southern armyworm (*Spodoptera eridania*)[1]. It is a non-enveloped T = 3 icosahedral insect virus of the family *Nodaviridae*. The PaV genome consists of two messenger-sense RNA molecules: RNA1 (3,011 nucleotides), which encodes protein A, the viral contribution to the RNA replicase; and RNA2 (1,311 nucleotides), which encodes protein α, the precursor to the viral coat proteins[2]. The 401 amino acid sequence of PaV protein α shares ~40% identity with the capsid proteins of the other insect nodaviruses (Fig. 1), whereas the RNA replicase of PaV is 26% identical to that of Flock House virus (FHV). These and other data indicate that PaV is the most distantly related member of the nodaviruses that infect insects.

Structural studies of two other nodaviruses, FHV and black beetle virus (BBV), placed them among the best understood icosahedral virus structures (for a review, see ref. 3). The nodavirus virus particle is an assemblage of 180 coat protein subunits that coencapsidate the two single-stranded genomic RNA molecules. Although the protein subunits are chemically identical, they occupy three quasi equivalent locations (A, B and C) within the icosahedral asymmetric unit (Fig. 2*a*). The A subunits form the 12 pentamers of the capsid whereas the B and C subunits alternate around the icosahedral three-fold axes to form 20 hexamers. The coat protein precursor α undergoes a post-assembly, self-catalyzed cleavage to yield mature coat proteins β and γ. This maturation is required for infectivity[4]. The portion of γ that is visible in the crystal structure (residues 364–381 in FHV) is helical in all known nodavirus structures and is thought to facilitate translocation of the viral RNA across host cell membranes during entry[5,6]. Despite this wealth of

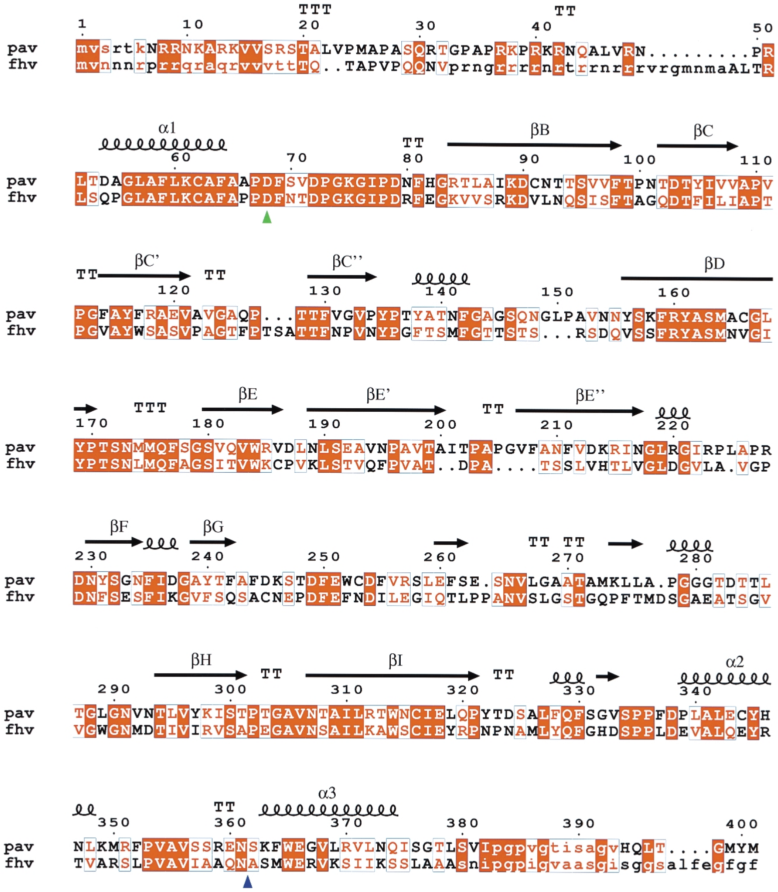

Fig. 1 Sequence alignment of PaV with FHV. Loops, arrows and T represent helix, β-strand and turns, respectively; their positions are based on the X-ray structure. Identical residues are shown as white text on a red background. Similar residues are shown as red text on a white background. Residues in lower case are those not visible in the PaV and FHV crystal structures. Blue and green arrowheads indicate the autocleavage site and the catalytically active residue respectively. This figure was adapted from ref. 2 and adjusted slightly based on the three-dimensional structures.

---

[1]Department of Molecular Biology, The Scripps Research Institute,10550 North Torrey Pines Road, La Jolla, California 92037, USA. [2]Department of Microbiology, University of Alabama at Birmingham, BBRB 373/17, 845 19th Street S, Birmingham, Alabama 35294, USA. [3]Department of Cell Biology, The Scripps Research Institute, 10550 North Torrey Pines Road, La Jolla, California 92037, USA. [4]Division of Cardiovascular Diseases, Scripps Clinic, 10666 North Torrey Pines Road, La Jolla, California 92037, USA.

Correspondence should be addressed to J.E.J. *email: jackj@scripps.edu*

© 2001 Nature Publishing Group http://structbio.nature.com

© 2001 Nature Publishing Group http://structbio.nature.com

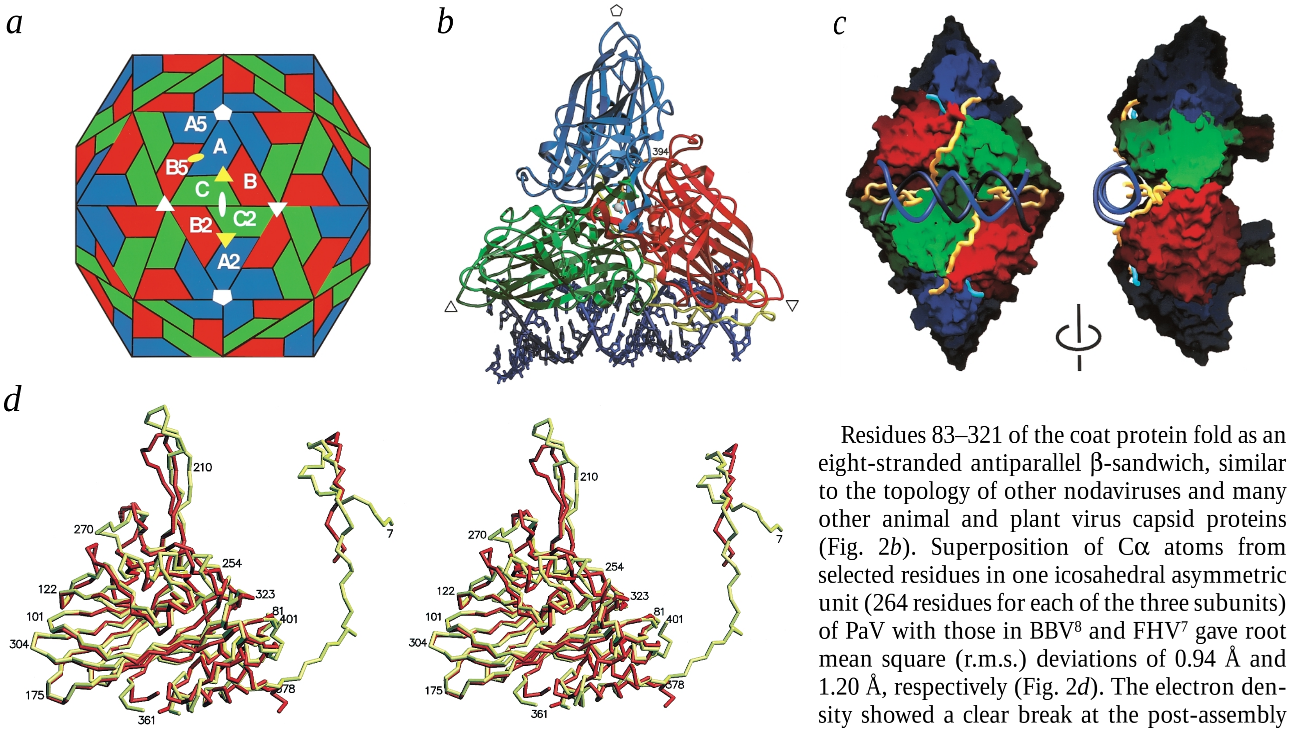

Fig. 2 The structure of PaV. ***a***, Schematic presentation of a T = 3 quasi equivalent lattice corresponding to a rhombic triacontahedron. Each trapezoid represents a single subunit (labeled A, B and C). The positions of the icosahedral two-fold, three-fold and five-fold axes are indicated by the white ovals, triangles and pentagons, respectively (yellow for local symmetry). A5, subunit A related by the icosahedral five-fold symmetry. ***b***, Overall structure of an icosahedral asymmetric unit of PaV (viewed from outside). Subunits A, B and C are colored blue, red and green, respectively. The extended N-terminus of subunit A is colored yellow and its C-terminus gold (residue 394 is labeled). The RNA duplex is shown as a stick model with coils through phosphorus atoms. Ca^{2+} is colored gray and the sulfate ion (which is mostly hidden behind the Ca^{2+} ion) cyan. The approximate positions of the three-fold and five-fold axes are indicated by triangles and a pentagon, respectively. The same color code is used hereafter unless otherwise stated. Figures were generated with Molscript[27], Bobscript[28], Raster3D[29] and GRASP[30]. ***c***, Left: the interior of the capsid showing the molecular surfaces of icosahedral asymmetric units related by the two-fold axis. Right: view rotated 90° relative to the left panel. The RNA duplex is shown as blue coils. The N-termini (residues 7–54) of the A subunits are colored yellow. Only the N-terminal portions of the eight-residue C-terminal segments (cyan) are seen. ***d***, Stereo view of the Cα superposition of subunit A of PaV (yellow) with FHV (red).

detail, studies of nodavirus structures have been frustrated by a lack of continuity of the polypeptide chains at the N- and C-termini of the subunits and by the visibility of only a short, 12-nucleotide RNA duplex represented by an island of density at the two-fold symmetry axes of the particle[7,8]. Here we report the crystal structure of PaV at 3.0 Å resolution and the electron cryo-microscopy (cryo-EM) image of PaV reconstructed at 23 Å resolution. The electron density reveals continuity of both RNA and the capsid protein that were not present in other nodavirus crystal structures.

Overview of the crystal structure

The crystal structure of PaV was determined by molecular replacement and real space averaging. The coordinates were refined to a crystallographic R-factor of 0.218 at 3.0 Å resolution with good stereochemistry. The present model of the asymmetric unit contains amino acid residues 7–378 and 394–401 of subunit A, 49–382 of subunit B, 51–382 of subunit C, a 25-nucleotide long RNA duplex, a calcium ion, a putative sulfate ion and 219 water molecules (Fig. 2*b*,*c*).

Residues 83–321 of the coat protein fold as an eight-stranded antiparallel β-sandwich, similar to the topology of other nodaviruses and many other animal and plant virus capsid proteins (Fig. 2*b*). Superposition of Cα atoms from selected residues in one icosahedral asymmetric unit (264 residues for each of the three subunits) of PaV with those in BBV[8] and FHV[7] gave root mean square (r.m.s.) deviations of 0.94 Å and 1.20 Å, respectively (Fig. 2*d*). The electron density showed a clear break at the post-assembly cleavage site between residues Asn 361 and Ser 362 for all three PaV subunits, consistent with the detection of protein γ in purified PaV[2]. Although the Asn-Ser sequence at the cleavage site differs from the Asn-Ala motif found in all other insect nodaviruses examined to date, the local structure around this site is very similar to that of BBV.

Residues 196–209 of three subunits join together around the quasi three-fold axis to form a ~15 Å protrusion at the surface (Fig. 2*d*). This is six residues longer in PaV than in FHV and BBV due to insertions between residues 200–208 (Fig. 1). The conformations of loops 144–154, 260–273 and 278–283 surrounding the protrusion in PaV are different from those in BBV and FHV. A single mutation in one of these surface loops in FHV (A265V, corresponding to Ser 264 in PaV) greatly reduced its infectivity of cultured *Drosophila melanogaster* cells[9], which are not susceptible to infection by PaV[2], suggesting that this region may be implicated in host cell recognition for the different virus species.

The C-terminus of subunit A

An 'island' of continuous density was observed in a channel near the quasi three-fold axis formed by subunits A, B and C of PaV. The density distribution agreed well with the sequence of the C-terminal eight residues (394–401) of protein γ. The average real space correlation coefficient between this segment in the refined model and the averaged electron density map was 0.83. We postulate that these eight residues extend from an A subunit that is related by five-fold symmetry to the A subunit contributing to the quasi three-fold axis close to the density (Fig. 3). There is weak density between the N-terminus of this eight-residue segment and the visible C-terminus of the five-fold related A subunit (A5). This weak density, while too diffuse to allow the preparation of a detailed model, is adequate to account for residues 379–393,

© 2001 Nature Publishing Group http://structbio.nature.com

© 2001 Nature Publishing Group http://structbio.nature.com

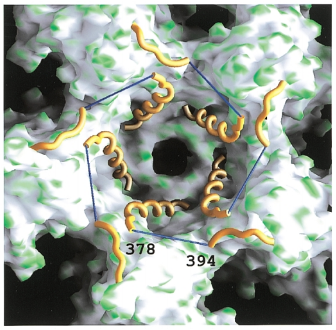

Fig. 3 The C-terminal segments. A view from the interior around the five-fold axis shows the arrangement of the C-terminal segments (gold stretches) and helices of γ polypeptides (gold) of the A subunits (molecular surface colored by curvature: concave, white; convex, green). Blue lines indicate the putative linkage between the amino end of the C-terminal segment (residue 394) and the carboxyl end of the γ polypeptide of a five-fold related A subunit (residue 378).

assuming that they are flexible. Thus, we conclude that the polypeptide chain forming subunit A5 extends at its C-terminus to interact with subunits A, B and C where they join at the quasi three-fold axis. The eight C-terminal residues lie deep in a channel formed by quasi three-fold related subunits A, B and C, with the C-terminal Met located nearly on the quasi three-fold axis (Fig. 2*c*). The C-terminal polypeptides interact via a remarkable nexus of hydrogen bonds, water bridges and van der Waals contacts with α2 helices (Fig. 1) and the visible N- and C-terminal portions of the three subunits around the quasi three-fold axis.

The extended N-terminus of subunit A

The extended N-terminal polypeptide of subunit A was clearly defined in the electron density map and was modeled starting from residue 7 (Fig. 4*a*). Proceeding from residue 54 to residue 7, the polypeptide leaves the region of the A subunit β-sandwich and passes along the bottom of the interface between subunits B and C (Fig. 2*c*). It continues into the groove at the inner surface of the protein shell that is formed by the two-fold symmetry-related asymmetric units adjacent to the RNA duplex. It extends along this groove, above the RNA and towards the icosahedral three-fold axis, interacting extensively with the proteins and the RNA duplex. Near the three-fold axis, the side chains of residues Ala 21 and Leu 22 contact their three-fold related counterparts to form a hydrophobic cluster with residues Met 174 and Met 175 of subunits B and C. The N-terminal polypeptide then turns back, and the visible N-terminal end inserts into the major groove of the RNA duplex (Fig. 4*b*). Residues 7–54 form extensive interactions with neighboring B and C subunits, resulting in the loss of solvent accessible surface areas of 1,405.5 Å^2, 643.5 Å^2 and 822.0 Å^2 for subunits B, C and a two-fold symmetry related C subunit, respectively. Electrostatic interactions dominate the contact between this segment and the RNA duplex. The N-terminus (residues 7–42) of the coat protein contains 12 basic residues, most of which are clustered around residues 11 and 40. Thus, a total of 24 basic residues from the N-terminal segments of A subunits from two icosahedral asymmetric units line up at the bottom of the groove to produce a positively charged environment that partly neutralizes the abundant negative charge of the RNA phosphate groups. Lys 61 of subunit C and Arg 370 of subunits B and C are also engaged in electrostatic interactions with the ordered RNA.

In many T = 3 plant viruses (for example, Southern bean mosaic virus[10] and Tomato bushy stunt virus[11]), the visible N-terminus of subunit C lies at the interface between asymmetric units related by icosahedral two-fold symmetry, extends to the icosahedral three-fold axis and contacts its three-fold related counterparts. The N-terminal segment in these viruses adds an extra β-strand to the canonical β-sandwich of subunit C to create a continuous β-sheet across the icosahedral two-fold symmetry related C subunits. Residues 22–33 of the N-terminus of the PaV A subunit occupy a similar position, although they lie below the β-sandwich and add no secondary structure to the interface.

The crystal structures of BBV[8] and FHV[7] revealed an island of density near the N-terminus that fit the amino acid sequence of residues 20–31 of the coat protein, but residues 1–19 and 32–54 were not visible. By analogy with the plant viruses, it was proposed that this polypeptide came from the

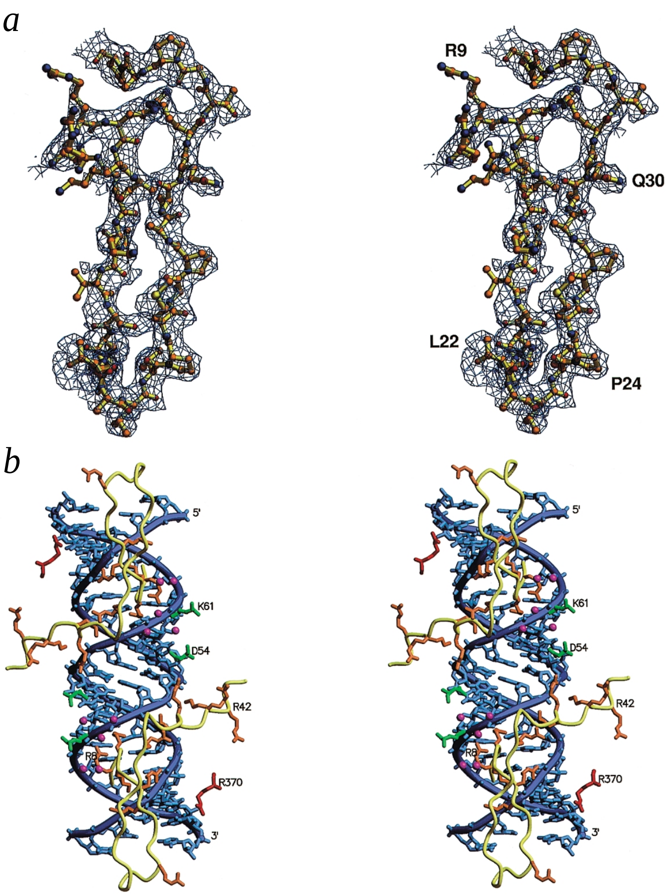

Fig. 4 The extended N-terminus of subunit A. ***a***, Stereo view showing the 60-fold averaged electron density map contoured at 0.7 σ superimposed with the refined model of the extended N-terminus of subunit A. ***b***, Stereo view showing the interactions between the N-termini of the A subunits (yellow) and the RNA duplex (blue). Basic residues from subunits A, B and C are colored orange, red and green, respectively. Side chains of Arg 8, Arg 9, Lys 11, Arg 13, Lys 14, Arg 37, Lys 38 and Lys 41 are in direct contact with the phosphate groups of the RNA duplex. Among them, Arg 8, Arg 9 and Lys 11 are in the major groove of the duplex. Other basic residues (Arg 18, Arg 31, Arg 40 and Arg 42) are close to the RNA duplex and also contribute to the overall positive charge. In addition, the guanidinium nitrogen atom of Arg 9 makes hydrogen bonds with N6 and N7 at the Hoogsteen edge of adenine 17 from a distance of 2.9 Å, and the guanidinium nitrogen atom of Arg 8 is 2.5 Å away from a phosphate oxygen atom of adenine 17.

© 2001 Nature Publishing Group http://structbio.nature.com

© 2001 Nature Publishing Group http://structbio.nature.com

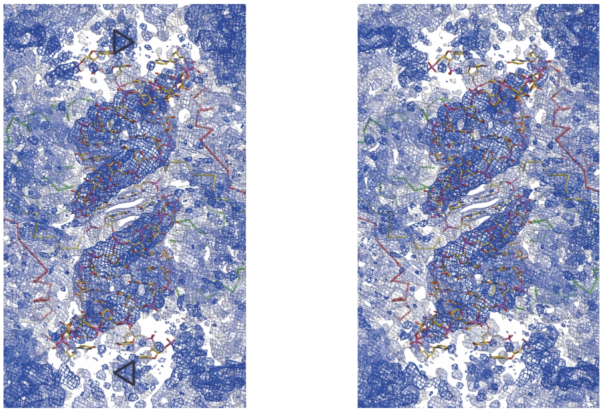

Fig. 5 Stereo view of the electron density of the RNA duplex. The electron density map (as in Fig. 4*a*) is contoured at 0.2 σ. The RNA duplex is shown as a stick model. The black triangles indicate the approximate positions of the icosahedral three-fold axes.

C subunit. In light of the PaV structure, however, it is highly probable that this polypeptide in BBV and FHV was in fact derived from the N-terminal region of the A subunit. In association with the RNA duplex, the N-terminal arm of subunit A functions as a molecular switch to maintain the flat interprotomer contacts that are critical for dimensioning the T = 3 particle. Mutation and deletion of residues 1–31 of the FHV coat protein caused the formation of virus-like particles that were heterogeneous in size and shape when expressed from a recombinant baculovirus[12].

The dodecahedral RNA cage

A 25-nucleotide long, A-type RNA duplex was modeled with high fidelity into the PaV electron density (Figs 4*b*,5). Density comparable to that of well-ordered protein was visible for the phosphate, sugar and bases of ribonucleotides 13–17, which lie closest to the icosahedral two-fold axes. Ribonucleotides 1–3 and 23–25 (at the ends) showed weaker but continuous density, consistent with the high temperature factors for the atoms of these ribonucleotides in the refined model. All sugars are assumed to be in the C3′ endo form and were modeled in that configuration. Nucleotides 14–17 were modeled as adenine while all others were modeled as uridine. Since the structure is averaged by icosahedral symmetry, the 25 ribonucleotides are an average of the true sequences that appear in each of the 30 unique segments. The good quality of the density reflects the high occupancy of icosahedrally equivalent volumes for all 30 duplexes. Nucleotides 13 and 14 of one strand form Watson-Crick base pairs with nucleotides 14 and 13 of the other strand. The base conformation of the other nucleotides appears relatively flexible as they do not form strict Watson-Crick base pairs. An overhang ribonucleotide at the 5′ ends of each strand lies close to the icosahedral three-fold axis. Near the three-fold axes, each of the two RNA strands extends towards the other strand of the equivalent duplex related by icosahedral three-fold symmetry in a tail-to-head manner. The three duplexes appear to form a three-way junction around the three-fold axis. As a result, all the ordered RNA duplex elements in the virus appear to form a dodecahedral cage (Fig. 6*c*). This cage provides an ‘averaged’ image of the organization of the ordered portion of the viral RNA. However, it is impossible for the RNA to adopt the three-way junction conformation at all 20 icosahedral three-fold axes because this would create 12 closed rings consisting of 125 ribonucleotides, which is inconsistent with the linear structure of the genomic RNA segments. The weaker density at both ends of the RNA duplex near the three-fold axes implies that adjacent duplexes are not always directly connected by their strands at the three-fold axes. Instead, the RNA chains sometimes connect to the bulk RNA, which must lie within the dodecahedral cage but does not follow the icosahedral symmetry. The 30 copies of the RNA duplex account for ~35% of the total viral genomic RNA (1,500 of 4,322 nucleotides).

The cryo-EM reconstruction

A three-dimensional cryo-EM reconstruction was obtained from the same virus sample used for crystallography (Fig. 6*a*). The resolution was better than 23 Å, as estimated by the Fourier shell correlation method. Characteristic surface features in this reconstruction show close similarity to the low resolution model calculated from the atomic coordinates of the crystal structure, for example, the protrusions at the quasi three-fold axes, the groove between the protrusions, and the shallow depression at the five-fold axes. The density of the reconstruction is layered at different radii: an outermost layer corresponding to the protein shell, a thin middle layer and a central core for RNA. Weak density connects these layers (data not shown). When contoured at a high level, the middle layer of density resolved into a dodecahedral framework as seen in the X-ray structure. A difference map was calculated by subtracting a low resolution model of the crystal structure without RNA from the reconstruction (Fig. 6*b*). The

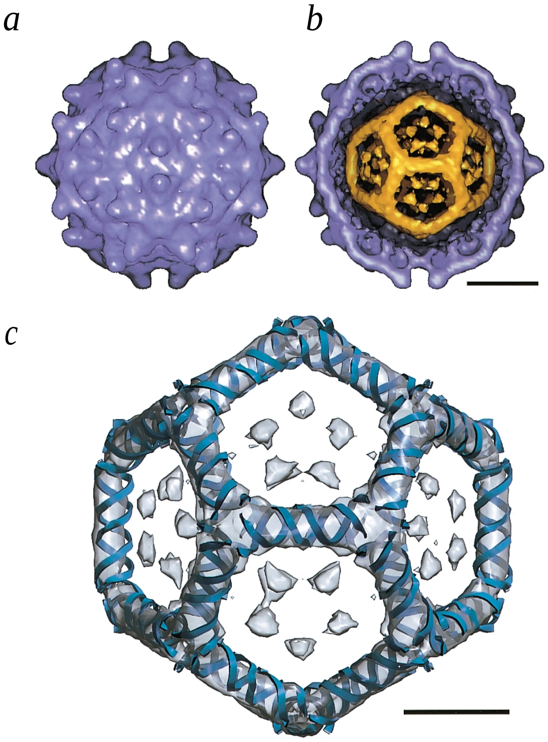

Fig. 6 Three-dimensional reconstruction of PaV. ***a***, The three-dimensional reconstruction of PaV contoured at 1.0 standard deviation above background viewed along the two-fold axis. ***b***, The difference map (gold) contoured at 4.2 standard deviations above background with the cutaway of the three-dimensional reconstruction. Bar = 100 Å. ***c***, The difference map (semi-transparent) superimposed on the RNA cage (blue ribbons) in the crystal structure. Bar = 50 Å.

© 2001 Nature Publishing Group http://structbio.nature.com

© 2001 Nature Publishing Group http://structbio.nature.com

same RNA framework emerged, and this is virtually superimposable with the RNA model from the crystal structure (Fig. 6*c*).

Table 1 Crystal structure determination and refinement

Data processing statistics			
Resolution (Å)	3.00–223.6	3.00–3.05	
Observations	3,226,875	136,241	
Unique reflections	1,505,825	76,058	
I / σ(I)	9.5	3.3	
Completeness (%)	81.2	82.2	
R_{merge}[1]	0.105	0.266	
Structure refinement statistics			
Resolution (Å)	20.0–3.0	3.14–3.0	
Reflections (F > 3σ)	1,237,980	101,838	
Completeness (%)	65.6	43.2	
R_{cryst}[2]	0.218	0.304	
R.m.s. deviations from ideal values			
	Protein	Nucleotides	
Bond lengths (Å)	0.008	0.003	
Bond angles (°)	1.457	0.708	
Dihedral angles (°)	28.470	15.791	
Improper angles (°)	0.733	1.286	
Temperature factor statistics (Å²)			
	<B>	B_{max}	B_{min}
Subunit A (7–378,394–401)			
Main chain	26.9	116.2	11.8
Side chain	28.8	118.8	6.5
Subunit B (49–382)			
Main chain	23.2	89.6	11.1
Side chain	23.8	91.2	7.9
Subunit C (51–382)			
Main chain	21.5	81.1	10.1
Side chain	22.6	82.7	5.2
Nucleotides (1–25)			
Backbone	178.7	229.8	86.8
Bases	175.2	229.1	89.0
Water (1–219)	27.7	74.8	3.7
Sulphate ion	189.5		
Calcium ion	39.0		

[1] $R_{merge} = \Sigma_h\Sigma_i|I_i(h) - \langle I(h)\rangle| / \Sigma_h\Sigma_i I_i(h)$, where $I_i(h)$ is the ith measurement of reflection h and <I(h)> is the average of all measurement of reflection h.

[2] $R_{cryst} = \Sigma_h|F_o(h) - kF_c(h)| / \Sigma_h|F_o(h)|$, where F_o and F_c are the observed and calculated structure amplitudes, respectively.

Conclusions

The crystal structure at 3.0 Å resolution and the low resolution cryo-EM reconstruction of PaV both reveal a dodecahedral cage of 30 RNA duplexes inside the icosahedral virus capsid. The ordered portion of PaV RNA is in close association with the inner surface of the protein shell, which shows remarkable complementarity to the RNA in both shape and electrostatic environment. The RNA close to the protein shell evidently adopts its highly ordered conformation through interactions with the capsid and thereby acquires the icosahedral symmetry that renders it visible at high resolution. In contrast, the remaining 65% of the viral RNA lies in the interior of the particle and does not adopt icosahedral symmetry even though it undoubtedly contains secondary structural elements. The weaker RNA density towards the ends of the duplexes suggests that the ordered RNA connects to the disordered regions primarily near the three-fold axes.

Studies of the structures and assembly of nodaviruses have shown that the viral RNA genome, by occupying the interface between capsid proteins related by two-fold symmetry, acts as part of a molecular switch that determines the geometry of the quaternary interactions required for T = 3 particle symmetry[7,12]. The remarkable organization of RNA duplexes seen in the structure of PaV now shows that the capsid exerts reciprocal influences over the three-dimensional arrangement of the viral RNAs.

Studies of FHV assembly have shown that the efficiency and specificity of RNA packaging are strongly influenced by the C-terminal sequence of protein γ, and in particular by the three Phe residues that lie at or near the C-terminus itself[13]. However, the crystal structures of FHV and BBV provide no insight into this aspect of assembly because the C-termini of all three quasi equivalent subunits are not visible in them[7,8]. The determinants of RNA packaging in PaV assembly remain to be explored, but it seems unlikely that the visible C-terminus of the A subunit could exert a direct influence on RNA packaging, at least from its final position in the mature virus particle. In contrast, the C-termini of the B and C subunits must lie somewhere in the icosahedrally disordered interior of the PaV particle, together with ~65% of the viral RNA and 48–50 amino acid residues from the N-termini of the B and C subunits. Many of the interactions that impose specificity on RNA encapsidation may occur in this location, where they would not be visible because they lack icosahedral symmetry.

The structure of PaV augments our current working model of nodavirus assembly[3]. Computational studies with BBV and FHV suggest that subunit trimers probably form first during assembly[14]. Since the A, B and C subunits are equivalent prior to further assembly events, the trimers will initially have three-fold symmetry. The N-termini of all three subunits are probably extended due to interactions in the interfaces, as observed for the A subunit of PaV. According to the model, the next step in assembly is the formation of pentamers of trimers that interact to form the bent contacts at the quasi two-fold axes. Pentamer formation breaks the three-fold symmetry and in so doing differentiates the A, B and C subunits. Pentamers of trimers are then thought to interact with RNA duplexes to form the flat contacts across the icosahedral two-fold axes. It seems reasonable to propose that the selectivity that accounts for the high specificity of RNA encapsidation is imposed at this step, perhaps by the binding of a particular RNA duplex with unusual properties (for example, a stem-loop with a particular sequence as observed in FHV[15]). Assembly could then be propagated by the less specific binding of other duplexes at successive two-fold axes to complete the dodecahedral cage. Although to date there is no definitive evidence for this assembly pathway, it is consistent with the energetics of subunit association and reminiscent of picornavirus assembly, for which experimental data clearly show that pentamers form first and then associate to create a pseudo T = 3 capsid[16].

The nodavirus structures demonstrate that the β-sandwich (residues 83–321) and the insertions between its strands function as a solid module, with little variation between quasi-equivalent subunits. The outer surface of this module controls interactions with the cellular receptor, while the functions of RNA encapsidation, quasi equivalent switching, autocatalytic proteolysis, and translocation of the genome across the cell membrane are all encoded at the termini of the capsid protein in

© 2001 Nature Publishing Group http://structbio.nature.com

© 2001 Nature Publishing Group http://structbio.nature.com

residues 1–82 and 322–401. The additional protein and RNA regions that are visualized in the structure of PaV have significantly expanded our understanding of the role of these components in the assembly and stability of virus particles.

Methods

Crystallization and data collection. PaV was purified as described[2] and crystallized by the hanging drop vapor diffusion method at room temperature. The reservoir was 1 ml of 75 mM Li_2SO_4, 5 mM $CaCl_2$ and 4% (w/v) PEG 8000 in 50 mM Tris-HCl buffer, pH 7.5. The droplet was a mixture of 1 µl reservoir solution and 1 µl virus sample at a virus concentration of ~20 mg ml^{-1} in 50 mM Tris-HCl buffer, pH 7.5. Crystals appeared within 4–5 days. The diffraction data were collected under cryo-conditions using 35% (v/v) ethylene glycol as the cryo-protectant. A data set at 3.5 Å resolution was collected on the BioCARS station 14 ID-B at the Advanced Photon Source (APS) and was used to compute an electron density map to determine an initial model. The refined structure reported here was based on 3.0 Å resolution data collected with a CCD detector at Beamline 9-2 of the Stanford Synchrotron Radiation Laboratory (SSRL) operating at a wavelength of 0.98 Å. A total of 239 images were collected with an oscillation angle of 0.5° and a crystal-to-detector distance of 275 mm. The data were processed with the program DENZO/SCALEPACK[17]. The crystal belonged to the $P2_1$ space group with cell parameters a = 329.3 Å, b = 346.9 Å, c = 424.9 Å and β = 90.8°. Data processing statistics are shown in Table 1.

Crystal structure determination and refinement. Molecular replacement and real space averaging were used to determine the crystal structure. The cell dimensions indicated that there was one virus particle in the asymmetric unit of the crystal. The approximate orientation of the particle in the unit cell was determined by a locked rotation function calculated with the program GLRF[18], and the particle center was located ~1/4 along both crystallographic *a* and *c* axes with an arbitrary position along the *b* axis of the polar space group. The accurate parameters of the particle position and orientation were determined by an iterative R-factor search using a polyalanine model based on the crystal structure of FHV[7]. The lowest R-factor was obtained when the PaV particle size was reduced by ~2.5% compared to the size of FHV determined at 20 °C. The polyalanine model was then placed in the unit cell according to the orientational and positional parameters to calculate an initial set of phases and an electron density map based on these phases and structure factor amplitudes from the PaV data. This 3.0 Å resolution map was subjected to cycles of phase refinement by 60-fold real space averaging with the programs RAVE[19] and CCP4 (ref. 20). An initial mask was created from the model with the program MAMA[21], and was edited during averaging to avoid truncation of density by the mask. The averaged map at the final cycle yielded an R-factor of 0.191 and a correlation coefficient of 0.901, and was readily interpretable.

The atomic model was built into the high quality, averaged electron density with the program O[22]. This model was subjected to multiple rounds of positional refinement, simulated annealing, overall B-factor refinement and restrained individual B-factor refinement with the program X-PLOR[23]. Geometric parameters were from slightly modified versions of PARHCSDX.PRO[24] for protein and DNA-RNA.PARAM[25] for RNA. A solvent mask was used as defined in X-PLOR. The refinement statistics are listed in Table 1. No outliers were found in the Ramachandran plot (87.1% in the most favored regions, 12.4% in the additionally allowed regions, 0.5% in the generously allowed region). The Cα superposition of the PaV structure with that of FHV was performed for residues 51–127, 129–144, 155–195, 213–222, 226–256, 284–358 and 363–376. The selection of compared residues was based on the sequence alignment and the three-dimensional structure. The correlation coefficient between the refined model and the electron density was calculated using RS-fit in the program O[22].

Electron cryo-microscopy. A droplet of 5 µl virus sample at ~1.5 mg ml^{-1} was applied for ~2 min onto a previously glow-discharged copper grid coated with a holey carbon film. The grid was blotted with preheated Whatman #2 filter paper to near dryness, flash frozen in liquid ethane, and then transferred into liquid nitrogen. Micrographs were recorded under low dose condition (~10 e $Å^{-2}$) on a Philips CM120 electron microscope operating at 100 kv with the grid maintained at ~100 K using a Gatan 626 cold stage. The objective lens was set to ~0.8 µm underfocus and the magnification was 45,000. Micrographs were digitized on a Zeiss SCAI scanner with a step size of 7 µm and averaged so that the pixel size of the final images was 4.67 Å. The best 69 images of boxed particles were used in the three-dimensional reconstruction with the program SPIDER[26]. A 20 Å resolution electron density map of a single virus particle was calculated from the atomic coordinates of the PaV crystal structure excluding RNA. Temperature factors of all atoms were set as 2,000 $Å^2$ to reduce the Fourier termination effect. This map was used as a reference to produce a set of projections with an angular interval of 2°. The images were aligned with these projections to determine the origins and orientations, and a three-dimensional reconstruction was calculated. Cycles of angular refinement were performed with an angular interval of 1.5° until convergence. Full icosahedral symmetry was imposed during the reconstruction.

To evaluate the quality of the reconstruction, the 69 images were divided into two groups, and two independent reconstructions were calculated. Fourier shell correlation and phase residual were computed between these two reconstructions. The resolution of the final reconstruction was estimated as ~23 Å where the Fourier shell correlation started to fall below 0.5 and the phase residual was ~70°. The average correlation coefficient between the raw images and the projections of the reconstruction was 0.35.

Coordinates. The atomic coordinates and the reflection file have been deposited with the RCSB Protein Data Bank (accession code 1F8V).

Acknowledgments
We thank the staff at The Stanford Synchrotron Radiation Laboratory (SSRL) and at the BioCARS sector of The Advanced Photon Source (APS) for help in data collection, M. Tihova and K. Dryden for help in electron microscopy, V.S. Reddy for stimulating discussion, and A. Palmenberg and J.-Y. Sgro for RNA secondary structure predictions. This work was supported by NIH grants to L.A.B., J.E.J. and M.Y. During this work M.Y. was an Established Investigator of the American Heart Association and Bristol-Myers Squibb and is now a recipient of a Clinical Scientist Award in Translational Research from the Burroughs Wellcome Fund.

Received 21 August, 2000; accepted 27 November, 2000.

© 2001 Nature Publishing Group http://structbio.nature.com

1. Zeddam, J.-L., Rodriguez, J.L., Ravallec, M. & Lagnaoui, A. A noda-like virus isolated from the sweet potato pest *Spodoptera eridania* (Cramer) (Lep.; *Noctuidae*). *J. Inv. Pathol.* **74**, 267–274 (1999).
2. Johnson, K.N., Zeddam, J.-L. & Ball, L.A. Characterization and construction of functional cDNA clones of Pariacoto virus, the first *alphanodavirus* isolated outside Australasia. *J. Virol.* **74**, 5123–5132 (2000).
3. Schneemann, A., Reddy, V. & Johnson, J.E. The structure and function of nodavirus particles: a paradigm for understanding chemical biology. *Adv. Virus Res.* **50**, 381–446 (1998).
4. Schneemann, A., Zhong, W., Gallagher, T.M. & Rueckert, R.R. Maturation cleavage required for infectivity of a nodavirus. *J. Virol.* **66**, 6728–6734 (1992).
5. Cheng, R.H. *et al.* Functional implications of quasi-equivalence in a *T*=3 icosahedral animal virus established by cryo-electron microscopy and X-ray crystallography. *Structure* **2**, 271–282 (1994).
6. Bong, D.T., Steinem, C., Janshoff, A., Johnson, J.E. & Ghadiri, M.R. A highly membrane-active peptide in Flock House virus: implications for the mechanism of nodavirus infection. *Chem. Biol.* **6**, 473–481 (1999).
7. Fisher, A.J. & Johnson, J.E. Ordered duplex RNA controls capsid architecture in an icosahedral animal virus. *Nature* **361**, 176–179 (1993).
8. Wery, J.-P., Reddy, V.S., Hosur, M.V. & Johnson, J.E. The refined three-dimensional structure of an insect virus at 2.8 Å resolution. *J. Mol. Biol.* **235**, 565–586 (1994).
9. Dasgupta, R., Selling, B. & Rueckert, R. Flock House virus: a simple model for studying persistent infection in cultured *Drosophila* cells. *Arch. Virol.* (Suppl.) **9**, 121–132 (1994).
10. Abad-Zapatero, C. *et al.* Structure of southern bean mosaic virus at 2.8 Å Resolution. *Nature* **286**, 33–39 (1980).
11. Harrison, S.C., Olson, A.J., Schutt, C.E., Winkler, F.K. & Bricogne, G. Tomato bushy stunt virus at 2.9 Å resolution. *Nature* **276**, 368–373 (1978).
12. Dong, X.F., Natarajan, P., Tihova, M., Johnson, J.E. & Schneemann, A. Particle polymorphism caused by deletion of a peptide molecular switch in a quasiequivalent icosahedral virus. *J. Virol.* **72**, 6024–6033 (1998).
13. Schneemann, A. & Marshall D. Specific encapsidation of nodavirus RNAs is mediated through the C terminus of capsid precursor protein alpha. *J. Virol.* **72**, 8738–8746 (1998).
14. Reddy, V.S. *et al.* Energetics of quasiequivalence: computational analysis of protein-protein interactions in icosahedral viruses. *Biophys. J.* **74**, 546–558 (1998).
15. Zhong, W., Dasgupta, R., & Rueckert, R. Evidence that the packaging signal for nodaviral RNA2 is a bulged stem-loop. *Proc. Natl. Acad. Sci. USA* **89**, 11146–11150 (1992).
16. Chow, M. *et al.* Myristylation of picornavirus capsid protein VP4 and its structural significance. *Nature* **327**, 482–486 (1987).
17. Otwinowski, Z. Data collection and processing. In *Proceedings of the CCP4 study weekend: data collection and processing* (eds Sawyer, L., Isaacs, N. & Baily, S.) 56–62 (Science and Engineering Research Council, Daresbury Laboratory, Daresbury, UK; 1993).
18. Tong, L. & Rossmann, M.G. The locked rotation function. *Acta Crystallogr. A* **46**, 783–792 (1990).
19. Jones, T.A. A set of averaging programs. In *Proceedings of the CCP4 study weekend: molecular replacement* (eds Dodson, E.J., Glover, S. & Wolf, W.) 91–105 (Science and Engineering Research Council, Daresbury Laboratory, Daresbury, UK; 1992).
20. Collaborative Computational Project, Number 4. The CCP4 suite: programs for protein crystallography. *Acta Crystallogr. D* **50**, 760– 763 (1994).
21. Kleywegt, G.J. & Jones, T.A. Halloween ... masks and bones. In *Proceedings of the CCP4 study weekend: from first map to final model* (eds Bailey, S., Hubbard, R. & Waller, D.) 56–66 (Science and Engineering Research Council, Daresbury Laboratory, Daresbury, UK; 1994).
22. Jones, T.A., Zou, J.-Y., Cowan, S.W. & Kjeldgaard, M. Improved methods for building protein models in electron density maps and the location of errors in these models. *Acta Crystallogr. A* **47**, 110–119 (1991).
23. Brünger, A.T. X-PLOR version 3.0 (Yale University, New Haven, Connecticut; 1992).
24. Engh, R.A. & Huber, R. Accurate bond and angle parameters for X-ray protein structure refinement. *Acta Crystallog. A* **47**, 392–400 (1991).
25. Parkinson, G., Vojtechovsky, J., Clowney, L., Brünger, A.T. & Berman, H.M. New parameters for the refinement of nucleic acid-containing structures. *Acta Crystallog. D* **52**, 57–64 (1996).
26. Frank, J. *et al.* SPIDER and WEB: processing and visualization of images in 3D electron microscopy and related fields. *J. Struct. Biol.* **116**, 190–199 (1996).
27. Kraulis, P.J. MOLSCRIPT: a program to produce both detailed and schematic plots of protein structures. *J. Appl. Crystallogr.* **24**, 946–950 (1991).
28. Esnouf, R.M. An extensively modified version of MolScript that includes greatly enhanced coloring capacities. *J. Mol. Graph. Model.* **15**, 132–134, 112–113 (1997).
29. Merritt, E.A. & Murphy, M.E.P. Raster3D version 2.0. A program for photorealistic molecular graphics. *Acta Crystallogr. D* **50**, 869–873 (1994).
30. Nicholls, A., Sharp, K.A. & Honig, B. Protein folding and association: insights from the interfacial and thermodynamic properties of hydrocarbons. *Proteins* **11**, 281–296 (1991).

© 2001 Nature Publishing Group http://structbio.nature.com